Nondestructive shape process monitoring of three-dimensional, high-aspect-ratio targets using through-focus scanning optical microscopy

OPEN ACCESS
IOP Publishing

Made open access 28 November 2018
Measurement Science and Technology

Meas. Sci. Technol. **29** (2018) 125007 (10pp)

https://doi.org/10.1088/1361-6501/aae4c2

Nondestructive shape process monitoring of three-dimensional, high-aspect-ratio targets using through-focus scanning optical microscopy

Ravi Kiran Attota[1,7], Hyeonggon Kang[1,5], Keana Scott[2], Richard Allen[3], Andras E Vladar[1] and Benjamin Bunday[4,6]

[1] Microsystems and Nanotechnology Division, NIST, Gaithersburg, MD 20899, United States of America
[2] Materials Measurement Science Division, NIST, Gaithersburg, MD 20899, United States of America
[3] Quantum Measurement Division, NIST, Gaithersburg, MD 20899, United States of America
[4] SUNY Poly SEMATECH, Albany, NY 12203, United States of America

E-mail: Ravikiran.attota@nist.gov

Received 15 June 2018, revised 18 September 2018
Accepted for publication 27 September 2018
Published 6 November 2018

Abstract

Low-cost, high-throughput and nondestructive metrology of truly three-dimensional (3D) targets for process control/monitoring is a critically needed enabling technology for high-volume manufacturing (HVM) of nano/micro technologies in multi-disciplinary areas. In particular, a survey of the typically used metrology tools indicates the lack of a tool that truly satisfies the HVM metrology needs of 3D targets, such as high-aspect-ratio (HAR) targets. Using HAR targets here we demonstrate that through-focus scanning optical microscopy (TSOM) is a strong contender to fill the gap for 3D shape metrology. Differential TSOM (D-TSOM) images are extremely sensitive to small and/or dissimilar types of 3D shape variations. Based on this, we here propose a TSOM method that involves creating a database of cross-sectional profiles of the HAR targets along with their respective D-TSOM signals. Using the database, we present a simple-to-use, low-cost, high-throughput and nondestructive process-monitoring method suitable for HVM of truly 3D targets, which also does not require optical simulations, making its use straightforward and automatable. Even though HAR targets are used for this demonstration, the similar process can be applied to any truly 3D targets with dimensions ranging from micro-scale to nano-scale. The TSOM method couples the advantage of analyzing truly isolated targets with the ability to simultaneously analyze many targets present in the large field-of-view of a conventional optical microscope.

Keywords: TSOM, nondestructive process control, three-dimensional metrology, through-focus scanning optical microscopy, nanometrology, nanomanufacturing, high-throughput semiconductor metrology

(Some figures may appear in colour only in the online journal)

[5] Current address: Coppin State University, Baltimore, MD 21216, United States of America.
[6] Current address: GLOBALFOUNDRIES, Malta, NY 12020, United States of America.
[7] Author to whom any correspondence should be addressed.

1. Introduction

With the increase in the use of three-dimensional (3D) structures in nano/micro technologies, high-throughput and economical 3D shape metrology and process monitoring of nanoscale to microscale objects is critically necessary [1–10]. This is technically challenging [4, 5, 7, 11–14], especially for high-aspect-ratio (HAR) targets, including through-silicon vias (TSVs) [13–18]. TSVs are a key component to enable 3D stacked integrated circuits (3DS-IC), which themselves are key to extended scaling of integrated circuits and enabling heterogeneous integration [15]. Hence it is crucial to find suitable metrology solutions for truly 3D targets such as HAR targets.

Several metrology tools are currently available or have been proposed [5, 9, 10, 19–41], for 3D shape measurements. Popular industrial metrology tools currently used are electron-based tools (e.g. scanning electron microscope (SEM)), probe-based tools (e.g. atomic force microscope (AFM)), and optics-based tools (e.g. scatterometers). The National Institute of Standards and Technology (NIST) pioneered the x-ray tool referred to as critical dimension small angle x-ray scattering (CD-SAXS) [31] that has attracted much attention from the semiconductor industry. Combination of the results of more than one measurement technique, referred to as either hybrid or holistic metrology, initially pioneered at NIST further improved nanometer-scale dimensional measurements [36, 42].

To be used in high volume manufacturing, a metrology tool must—in addition to providing statistically significant results [12]—be fast (high-throughput), low-cost, inline capable, automated, robust, easy to use, non-contact and non-destructive. The requirements for satisfactory measurement sensitivity and resolution have been identified in the International Technology Roadmap for Semiconductors (ITRS) [43] and International Roadmap for Devices and Systems (IRDS) 2017 Edition: Metrology [44]. All currently available tools have certain advantages and disadvantages. It is difficult to find a metrology tool that satisfies all the abovementioned requirements, especially for metrology of 3D/HAR targets.

It is very difficult to use top-down SEM imaging for 3D shape analysis of HAR targets at high-throughput with sufficient measurement resolution. Probe-based tools, such as AFM, have limitations in reaching the bottom of HAR targets due to probe length and width constraints and generally do not meet high-throughput requirements. CD-SAX tools currently are too expensive to be industrially relevant for high-volume manufacturing (HVM). Among non-destructive metrology tools traditionally used in nano/micro technologies, optical tools are usually better suited for inline metrology applications. Optical tools, such as spectral reflectometry [35] and interferometry [16] are available for high-throughput depth measurement of HAR targets but are not capable of determining 3D shape. The workhorse of the semiconductor industry, scatterometry, is another optics-based technique widely used for measurement of shallow repeated structures, but is limited in its ability for 3D shape analysis of deeper and/or isolated HAR targets [13]. Model-based infrared reflectometry (MBIR) technique is reported to measure depth, top and bottom critical dimensions of TSVs and HAR targets [45]. But the MBIR technique also relies on simulations similar to scatterometry and is limited in its ability for dimensional analysis of individual HAR targets. There seems to be a gap in HVM metrology tools for complete shape analysis of truly 3D or HAR targets. It would be advantageous if the tool also does not rely on optical simulations.

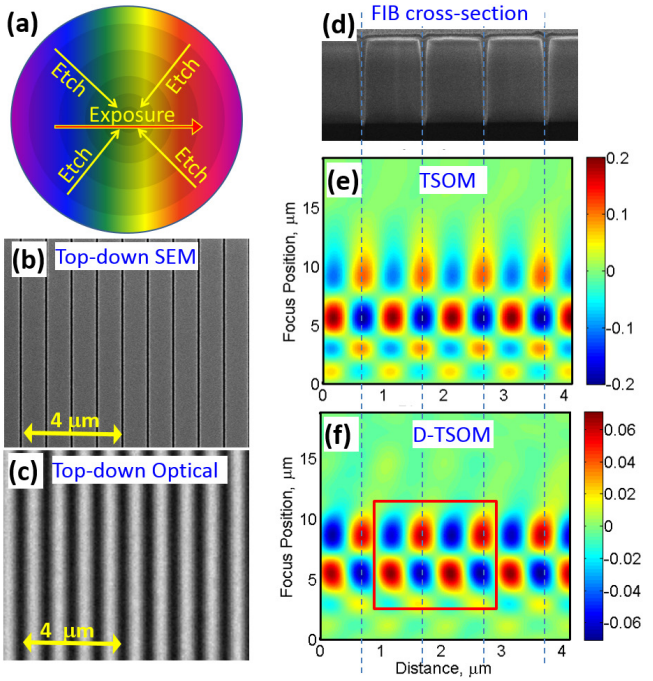

Figure 1. (a) Exposure and etch conditions used to fabricate the HAR wafer. Exposure time increases from left to right. Etching changes radially, being slower at the edges. Typical (b) SEM, (c) optical, (d) dual-beam FIB etched cross-sectional SEM, (e) TSOM, and (f) D-TSOM images. The color scale bars in (e) and (f) represent the optical intensity. Nominal pitch = 1000 nm. Optical data acquisition conditions $\lambda = 520$ nm, numerical apertures (NA) = 0.75, illumination NA (INA) = 0.25.

We demonstrate here how a NIST-developed optics-based metrology tool, through-focus scanning optical microscopy (TSOM) [18, 43, 44, 46–55], could fill this gap. The TSOM image is generated from a set of images, each captured at a slightly different focus (i.e. through-focus), using a low-cost, conventional optical microscope. Thus, TSOM collects and preserves the entire through-focus optical intensity information in 3D space. The collected set of through-focus two-dimensional optical images are then stacked at their respective focus positions creating a 3D space filled with the optical intensities. From this 3D space, extracting and plotting the optical intensities in a vertical cross-sectional plane results in a TSOM image. In the TSOM image, the *X* and the *Y* axes represent the distance and the focus positions, respectively. The color represents the optical intensity. A TSOM image depicts variations in the optical intensities with focus position. The color pattern enables visualization of the variations in the optical intensities easily. The TSOM images were then normalized [52, 56, 57]. The normalization procedure nearly eliminates the effect of variations in the experimental

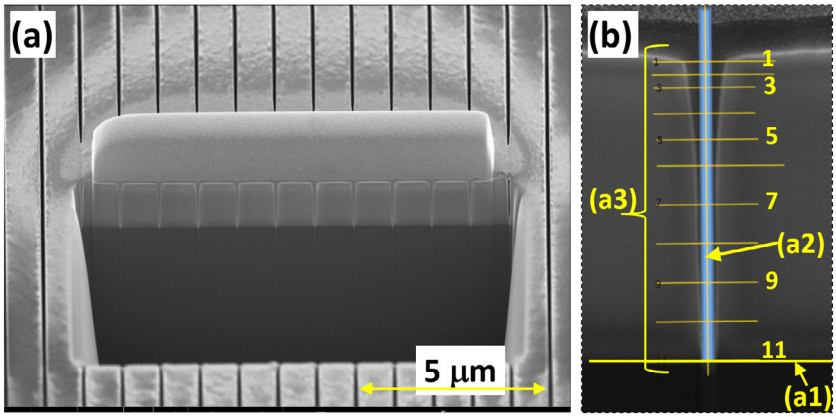

Figure 2. (a) A typical FIB cross-sectional image. (b) A typical high-magnification cross-sectional image with horizontal lines at the depths at which profile measurements were taken (a3).

conditions such as the illumination source intensity, camera exposure time, frame rate. However, it is advisable to optimize conditions to reduce noise [57, 58].

D-TSOM images are generated by taking a pixel-by-pixel difference between two TSOM images obtained using two different targets. D-TSOM images expose small (down to sub-nanometer) differences embedded in nominally identical targets. The color patterns of D-TSOM images are usually distinct for different types of parameter changes and serve as a 'fingerprint' for different types of parameter variations. D-TSOM images are qualitatively similar for different magnitude changes in the same parameter. However, the optical content of D-TSOM images is proportional to the magnitude of the dimensional differences. We developed a metric we call the optical intensity range (OIR), which provides a quantitative estimate of the difference between two images. The OIR is the absolute optical range (i.e. the difference between the maximum and the minimum optical intensity) of the D-TSOM image, multiplied by 100 [52, 56]. The utility of D-TSOM [18, 47, 52, 53, 59] is that the color pattern of the D-TSOM image is an indicator of the difference in 3D shape, while the magnitude of the OIR scales with the dimensional difference between the two targets. Developments in image acquisition techniques have significantly reduced the acquisition time for a set of through-focus images to be as fast as a single conventional microscope image [50, 54, 60–62] making TSOM suitable for HVM.

Here we present a comprehensive study that demonstrates the applicability of TSOM for shape analysis of truly 3D trench targets with HAR. We show that the scattered light, which could be due to multiple scattering, contains the 3D shape information. TSOM facilitates extraction of this useful information and allows us to propose a simple, cost-effective, non-destructive, 3D shape process control method.

2. Methods

2.1. HAR target fabrication

The current work uses a 300 mm silicon wafer with HAR targets in a SiO_2 layer. First, a 1.1 μm thick SiO_2 film was deposited on the silicon wafer. HAR features covering an area of 150 μm × 150 μm were etched into the oxide film with a nominal CD, depth and pitch of 100 nm, 1100 nm and 1000 nm, respectively. Exposure and etch conditions were varied across the wafer, as shown in figure 1(a), to provide slight variations in the feature structural parameters. This provides a systematic dimensional variation in the HAR targets across the wafer. Typical SEM and optical images are shown in figures 1(b) and (c), respectively.

2.2. FIB cross-section

Cross-sectional analysis of the HAR targets was performed using a focused ion beam scanning electron microscope (FIB SEM) equipped with a gas injection system. First, the HAR target areas were filled with Pt using the primary electron beam at 10 keV landing energy and with 1.6 nA beam current at 0° sample stage tilt. Once the targets were filled in, additional 1 μm thick Pt layer was deposited using the 30 keV, 800 pA ion beam. This layer was deposited to protect the sample surface during the cross-sectioning steps. Rough milling to remove the bulk of the material was performed at 2.5 nA ion beam current. The exposed cross-sectional face was further cleaned with a lower ion beam current (0.79 nA) fine milling. The cross-sectional face was imaged using a 2 keV, 100 pA electron beam with a through-the-lens detector (TLD) in immersion mode. A typical cross-sectional image thus obtained is shown in figure 1(d).

The following procedure was used to determine the precise cross-sectional profiles of the HAR targets. A typical large-area FIB cross-sectional image is shown in figure 2(a). A highly magnified cross-sectional profile of a single HAR trench is shown in figure 2(b). A line was first drawn along the SiO_2–Si interface at the bottom ((a1) in figure 2(b)). A perpendicular line (blue wide bar with a yellow central line) was drawn to this boundary passing through the middle of the trench at one-third of the distance from the top ((a2) in figure 2(b)). Eleven horizontal lines were drawn at the predefined depths covering the entire depth of the trench ((a3) figure 2(b)). Distances of the left and right profiles from the central vertical line were then carefully measured at the 11

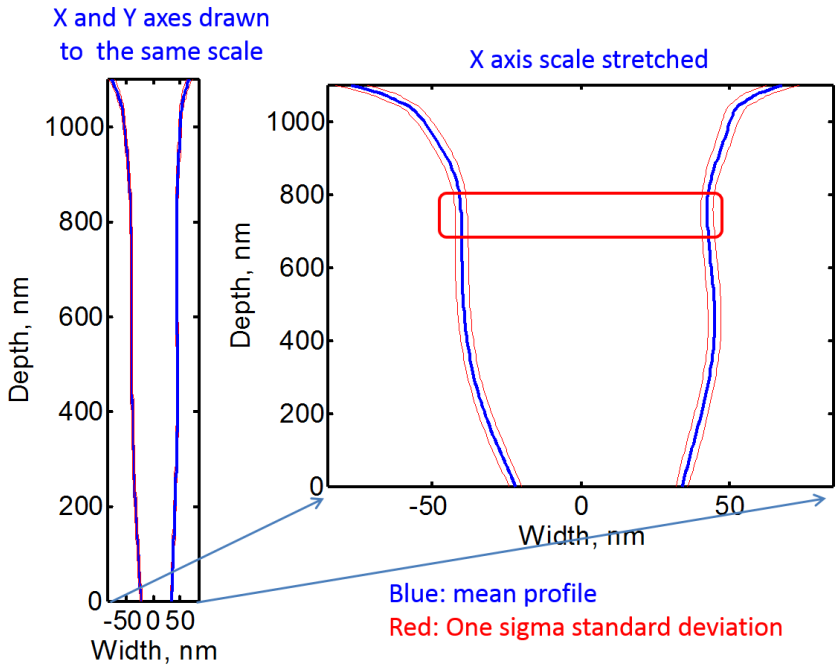

Figure 3. Measured mean cross-sectional profile of the target in the central die. Red profiles indicate mean standard deviations of all the profiles.

horizontal line locations, providing the cross-sectional profile of the trenches. A cubic spline fit was drawn through the 11 points on the left and the right separately resulting in the left and right profiles. For each die, a minimum of six such profile measurements were made on six different trenches. The final cross-sectional profile is a mean of these six measurements. The mean cross-sectional profile obtained in such a manner is shown in figure 3 (blue profile) for the central reference die along with the standard deviation which is shown as red profiles. The lowest measured cross-sectional profile standard deviation was observed at about one-third of the depth from the top as highlighted by a red box in the graph with the expanded x-scale, on the right of figure 3.

2.3. TSOM Experiments

A commercially available conventional, bright-field optical microscope in the reflection mode was used to collect the TSOM images. The optical microscope was designed for Kohler illumination. A light-emitting diode (LED) was used as an illumination source. A narrow, band-pass filter was used to obtain an illumination wavelength of 520 nm (±5 nm). TSOM images were captured using a 40x magnification objective with 0.75 numerical aperture (NA) and 0.25 illumination NA. An image of approximately 55 μm × 40 μm was captured using a cooled, monochrome CCD camera (692 x 520 pixels). A width of 0.5 μm (along the trenches) of the image at the center of the field-of-view (FOV) was averaged to obtain a mean intensity profile. From this, 2 μm length (across the trenches) at the center of the extracted profile was used from all of the through-focus images to construct the TSOM images. A through-focus step height of 300 nm, and a total through-focus scan range of 25 μm was used to collect the set of through-focus images. The experimental data were collected using 0° illumination polarization (*E*-field perpendicular to the trenches) which provided higher sensitivity. Other typical processing conditions used and the effect of optical parameters can be found in [56, 57]. The through-focus optical images forming the 3D optical data set were analyzed using an in-house developed software program.

TSOM data were collected at the center of the target. Three sets of TSOM data from the 80 usable dies across the wafer were collected. For this work, we considered the target in the center die (0,0) as the reference. The TSOM image processing and normalization procedure can be found in earlier publications [56, 57]. An example of one TSOM image is shown in figure 1(e). D-TSOM images were evaluated by subtracting the TSOM image of the reference target from each of the TSOM images associated with the targets in the other 80 dies. A typical D-TSOM image is shown in figure 1(f); note the scale on the color bar as compared to that of figure 1(e).

3. Results and discussion

3.1. TSOM data

Even though we expect to see variation between the targets due to the process variation shown in figure 1(a), the color patterns for the TSOM images appear to be nearly identical for all the targets on the different dies. In contrast with the TSOM images, the color patterns of the D-TSOM images vary substantially based on the die selected. Typically, a sub-section of the D-TSOM image as highlighted by a red rectangle in figure 1(f) contains the strongest color pattern. Hence, we selected this sub-section (maintaining the same focus and distance ranges) from all the D-TSOM images and created

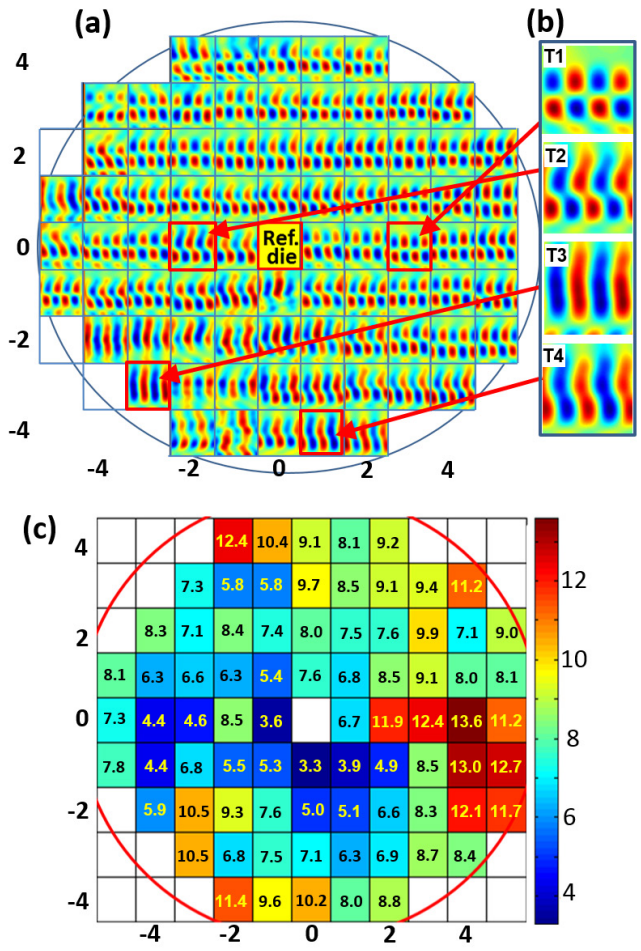

Figure 4. TSOM results. (a) A mosaic of the D-TSOM images obtained by subtracting the TSOM image of the central reference target from the TSOM images of the targets in the other dies with color scale bar set to automatic. (b) Four major types of D-TSOM image color patters identified. (c) OIR values of the D-TSOM images representing the automatic color scale ranges in (a). Standard deviations of these OIR values varies between 2% to 10%, with the majority of them falling below 5%. Each die can be uniquely identified using the assigned co-ordinates in (a) and (c).

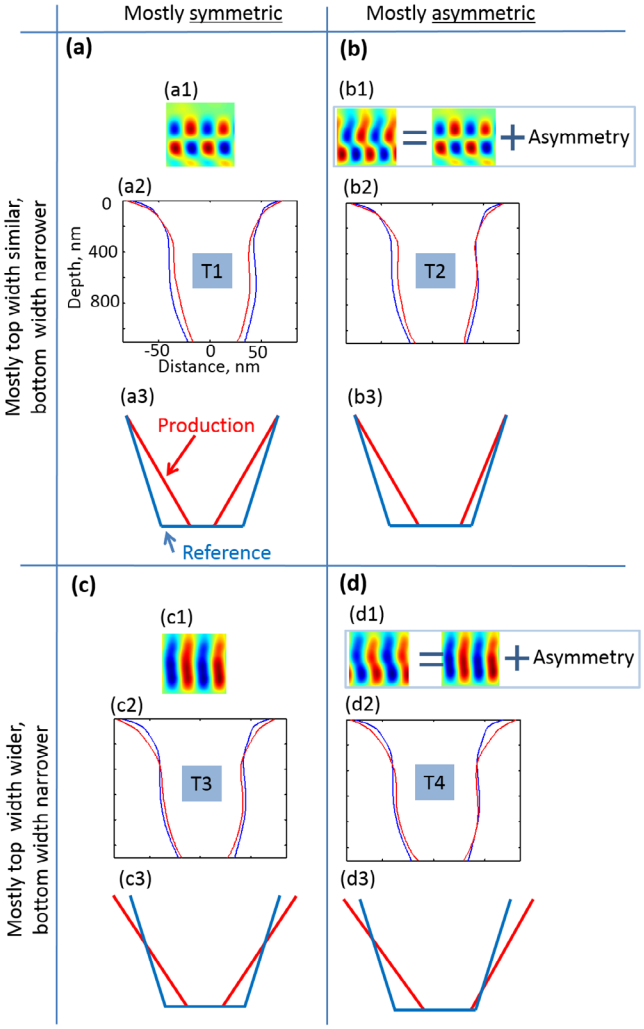

Figure 5. A summary showing four major D-TSOM images (a1)–(d1), their corresponding FIB-cross sectional shape profiles (a2)–(d2) and types of simplified shapes (a3)–(d3) represented as T1, T2, T3, and T4 in (a)–(d), respectively. In (a2)–(d2) the blue color profile is from the reference target, while the red color profile is from the production target. Different types of 3D profile differences between the reference and the production targets result in D-TSOM images with different color patterns.

a mosaic of the D-TSOM images by placing them in their respective die locations covering the entire wafer as shown figure 4(a). Please note that these D-TSOM images are set to automatically scale the color to highlight the color patterns.

At a first glance, the D-TSOM image color patterns appear to be varying widely. However, careful observation shows that they are mostly variations of the four basic color patterns (T1, T2, T3 and T4) as identified in figure 4(b). Figure 4(c) converts the ranges of optical strength in the D-TSOM images into OIR values, which are set at their respective die locations.

One can see that the upper semicircle of figure 4(a) is mostly filled with T1 or T2 types of 3D shape differences and the lower semicircle is mostly filled with T3 or T4 types of differences. Further, the larger OIR of the D-TSOM images on the right side of the semicircle in figure 4(c) indicates larger dimensional difference targets compared to the left side of the semicircle. While these observations suggest how much the different HAR structures vary, one needs additional information to know what type of shape or dimensional differences the T1, T2, T3 and T4 type of D-TSOM images represent.

3.2. 3D profile analysis with TSOM

For the purposes of this analysis, we compared information collected using D-TSOM and FIB-SEM cross-section. After comparing the cross-sectional profiles of the selected reference targets, a correlation between the D-TSOM images and the geometry was identified. A summary of this correlation is presented in figure 5. The four typical types of D-TSOM images identified in figure 4(b) can be correlated with the following cross-sectional characteristics.

- Type T1 D-TSOM image (figure 5(a1)). It is associated with mostly symmetric profile differences from top to bottom, with nearly similar width at the top but narrower width of the production target at the bottom (figure 5(a2)). Schematically we can represent this type of difference as shown in figure 5(a3).
- Type T2 D-TSOM image (left part of figure 5(b1)). It is associated with mostly asymmetric profile differences

from top to bottom, with nearly similar width at the top but narrower width of the production target at the bottom (figure 5(b2)). Schematically we can represent this type of difference as shown in figure 5(b3). Since the profile differences are similar to figure 5(a2), except with asymmetry, we can propose that T2 type of D-TSOM image is a result of T1 type of profile differences with some asymmetry present. This is presented in figure 5(b1).

- Type T3 D-TSOM image (figure 5(c1)). It is associated with mostly symmetric profile differences from top to bottom with production target wider at the top but narrower at the bottom (figure 5(c2)). Schematically we can represent this type of difference as shown in figure 5(c3).
- Type T4 D-TSOM image (left part of figure 5(d1)). It is associated with mostly asymmetric profile differences from top to bottom, with the production target wider at the top but narrower at the bottom (figure 5(d2)). Schematically we can represent this type of difference as shown in figure 5(d3). Since the profile differences are similar to figure 5(c2), except with asymmetry, we can propose that T4 type of D-TSOM image is a result of T3 type of profile differences with some asymmetry present. This is presented in figure 5(d1).

3.3. Process monitoring with TSOM

From these results, we identify two paths to the desired fast, low-cost, inline capable, automated, robust, easy to use, non-destructive and statistically significant metrology tool for a high-volume production environment. For the sake of argument, we can consider the target in the central die (the reference target (0,0)) as an ideal target with desirable dimensions. In a production environment, this information would be available from a 'golden' standard or reference. We consider the targets in the rest of the dies as exhibiting dimensional variations, as it would be typical in production.

3.3.1. First approach. As the first approach, we propose using only the OIR values for the process monitoring. In earlier work, we showed that the magnitude of the OIR increases with the magnitude of the dimensional difference [18, 47, 52] between the reference and target under test. Thus, in production we can identify a maximum OIR value for an acceptable production target, for which, when exceeded, an unacceptable percentage of the related devices will fail.

This first approach is an example of high-throughput and quick way of using TSOM as a simple 3D shape process monitoring method. However, it has the drawback of not identifying the type of dimensional difference the D-TSOM image represents. Since there are several types of D-TSOM image color patterns in figure 4, we can expect many types of 3D shape deviations from the reference target. From the OIR alone we are unable to single-out deviation in the dimension that is critical (usually called the critical dimension) for the application. A small deviation in the critical dimension may not be acceptable, whereas a larger deviation in a non-critical dimension may be acceptable. If the process monitoring is done purely based on the OIR values, there is a possibility that useable targets may be rejected if the high OIR value of a D-TSOM image is a result of a large non-critical dimensional difference, and vice versa.

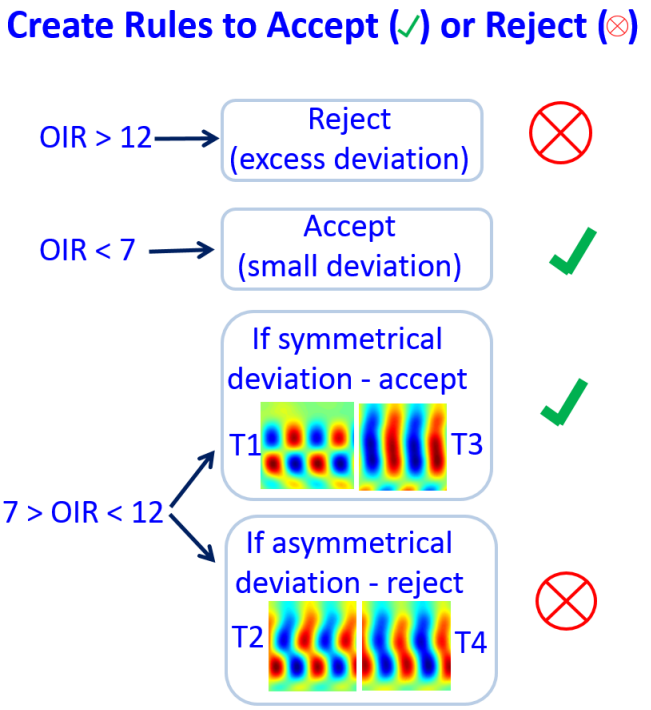

Figure 6. Process control rules arbitrarily selected for demonstration purposes.

3.3.2. Second approach. The second course of action allows us to make intelligent process monitoring decisions with enhanced accuracy using the knowledge gained by determining the correlation between the color pattern in the D-TSOM image and the type of dimensional difference. This analysis needs determination of the complete 3D shape of targets corresponding to specific families of TSOM images. This process is similar to the library development in scatterometry, which is widely used in high-volume manufacturing. However, in the TSOM method we make use of experimentally generated library where as in the case of scatterometry optical simulations are used. For this work we developed such a library using the FIB SEM cross-sectional images described above and shown in figure 3, as well as those having similar patterns but exhibiting a range of OIR values. The D-TSOM images and the evaluated profile correlations become a library for the second approach.

Equipped with the information and correlations identified in figure 5, we then propose the following steps for 3D shape process control of the HAR targets.

- At first, we create accept/reject rules. These rules should be based on the process control requirement. For the sake of demonstration, we have created the following rules randomly (these rules are shown graphically in figure 6). If the OIR of the D-TSOM image is more than 12, reject the target as the dimensional differences are in excess of the tolerable limits. On the lower side, if the OIR of the

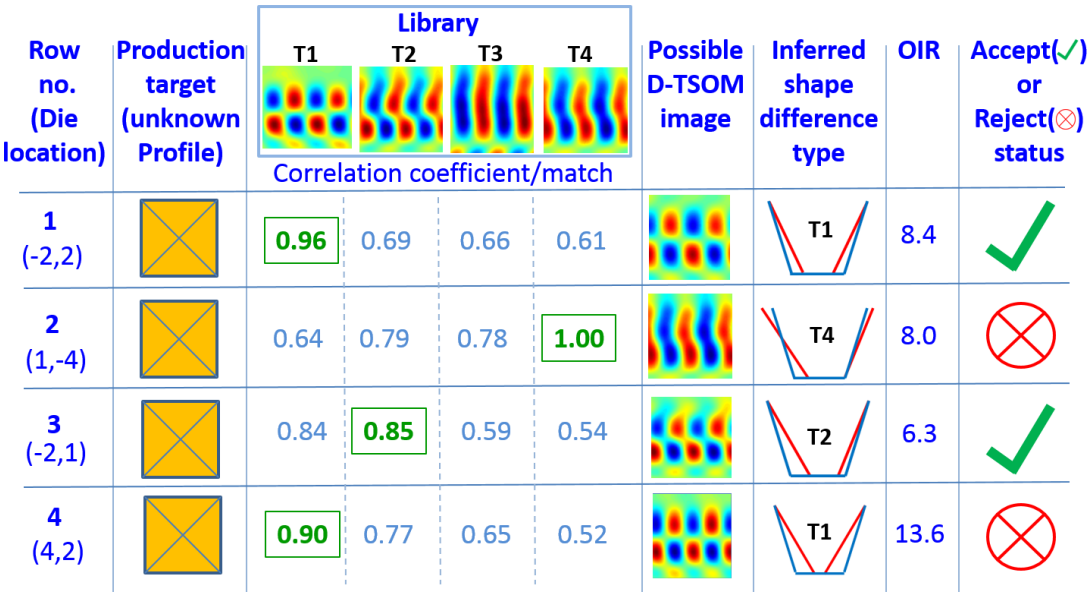

Figure 7. Proposed TSOM-based automated 3D-shape process control method. The selected test production targets in column 1 are considered to have unknown 3D-shape profile (column 2). Comparing the D-TSOM images of the test targets with the library provides the best match (green boxes) from which the possible 3D shape difference type can be inferred (column 8). Based on the type of 3D shape difference and the magnitude of the dimensional difference (OIR), the process control decision of accept/reject status can be made.

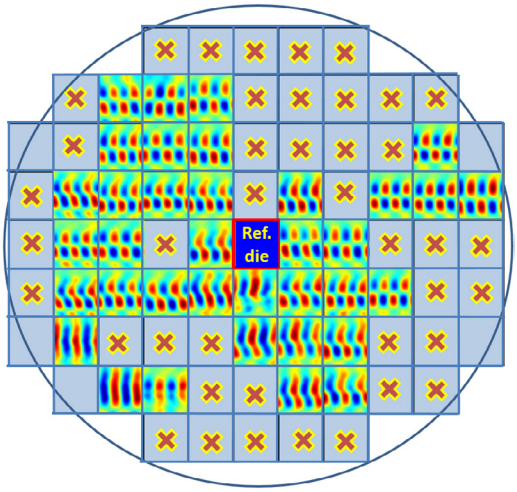

Figure 8. Dies marked by an X are rejected after applying the automated TSOM-based process control criteria of figure 7 to the entire wafer shown in figure 2, using the created rules (figure 6). The rest of the dies are deemed acceptable.

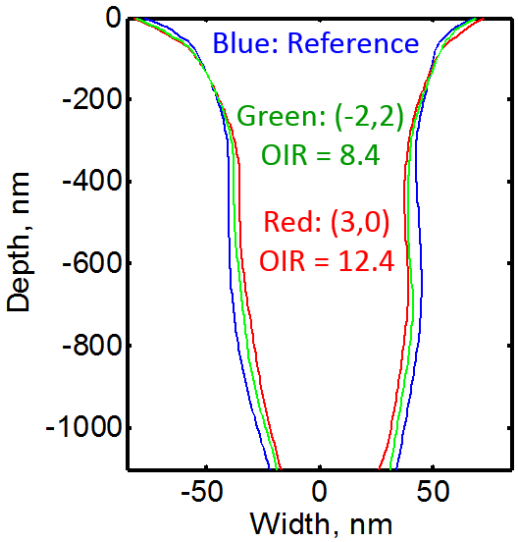

Figure 9. Cross-sectional profiles overlaid for targets from the reference die (blue profile), die (−2, 2) (green profile), and die (3, 0) (red profile).

D-TSOM image is less than 7, accept the target as the dimensional differences are within the acceptable level. If the OIR value is in between 7 and 12, reject the production target if the profiles are asymmetric and accept if the profiles are symmetric.

- Now consider a random production target, for example the one located at position (−2,2) in figure 4. Initially, we have no knowledge of the type of target shape deviation from the reference target. Since its OIR value is 8.4, we then proceed to the next step where its D-TSOM image is compared with the reference library to determine which D-TSOM image from the library matches best with it. This target shows highest correlation with type T1 D-TSOM image; this can be determined by calculating the correlation coefficients by comparing the D-TSOM image with each reference image in the library. In this case, the best correlation of the target at (−2, 2) is with the type T1 (figure 5(a)). Since this target has a mostly symmetric shape difference and its OIR value is less than 12, the final verdict is 'Acceptable'. Figure 7 illustrates this decision process as row number 1. We can unambiguously bin (accept/reject) the unknown targets at positions (1, −4), (−2, 1), and (4, 2), following the similar decision process as depicted in rows 2, 3, and 4, respectively, using only the OIR values and the correlation coefficients.

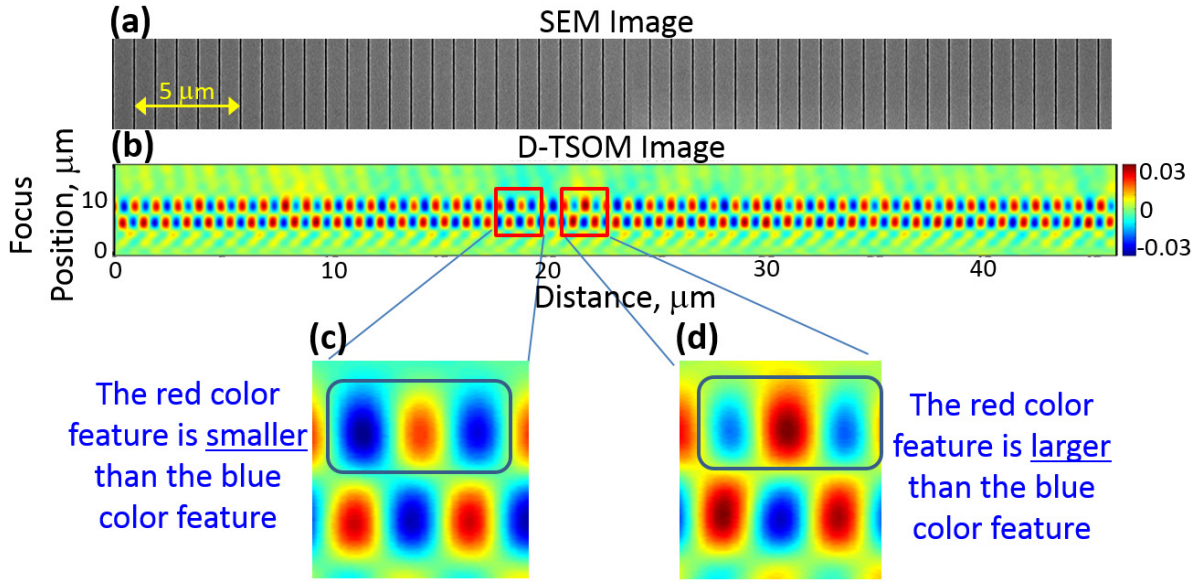

Figure 10. Large area analysis using TSOM. (a) A typical top-down SEM image of a 50 μm long HAR sample. (b) D-TSOM image obtained using die (3,1) and the reference die. (c) and (d) Magnified areas highlighted by red boxes in (b) showing differences in the localized color patterns.

The unknown target in row 3, (−2,1), has the highest correlation coefficient with T2. However, its correlation coefficient is also close to type T1. Similar, but still-high correlation with T1 and T2 indicates that the unknown target is type T1 with asymmetry, i.e. type T2. Since correlation coefficients derived from D-TSOM images and OIR values are all numerical values, the decision process is simple and can easily be automated. The remaining acceptable dies after applying the selected process control rules to the wafer shown in figure 4 ARE presented in figure 8.

3.3.3. Verification of the 3D shape analysis. Here we present a test case to verify the accuracy of the TSOM method of process control (figure 9). We chose two die locations (−2, 2) and (3, 0) that show type T1 D-TSOM images but with different magnitude of OIR values of 8.4 and 12.4, respectively. Since both the dies have type T1 profile differences, their cross-sectional profile differences should be similar when compared to the reference profile. However, the target in die (3,0) with a higher OIR value should have a larger profile difference compared to the target in die (−2, 2). Measured FIB cross-sectional profiles shown in figure 9 support this, i.e. a larger difference in the profile results in a larger OIR, validating the analysis made by the TSOM method.

3.3.4. Large area and intra-die analysis. The TSOM method can also be used to identify anomalies in targets covering a large area. In figure 10, we present 50 μm long HAR sample SEM (figure 10(a)) and D-TSOM (figure 10(b)) images. While the D-TSOM image pattern typically matches with type T1, which is mostly symmetrical profile differences, some local variations can be identified. We highlighted two of the several local variations in the D-TSOM image by the red boxes. In figure 10(c), the red color area between the two blue color regions is less dominant in the highlighted blue box, whereas in figure 10(d), it is more dominant. This difference is a result of the underlying localized cross-sectional profile (i.e. 3D) shape differences. Even though at present it is not known what type of profile differences result in this type of D-TSOM images, this demonstrates the ability of the TSOM method to highlight them easily. A further finer localized FIB-cross sectional analysis would reveal the underlying profile shape differences precisely. A similar process can also be applied to identify dimensional variations within a die. In this way, localized variations (or defects) within a large area that fits in the FOV of a microscope can be identified simultaneously using the TSOM method.

TSOM has unique advantages over other metrologies such as scatterometry, as it can be used to independently analyze every 3D structure (such as the HAR target demonstrated here); and over metrologies such as SEM, as it can be used to simultaneously analyze a large number of targets present in a large field-of-view (FOV) of a microscope with measurement resolution comparable to SEMs and AFMs. TSOM can also be used to study dimensional variations within a die, not possible with either scatterometry or MBIR. It is also not possible to obtain 3D shape information using SEM non-destructively, and measure narrow spaces using AFM due to probe size limitations. In the case presented here we have demonstrated that TSOM does not have these two limitations.

This paper demonstrates the basic 3D shape process control procedure using the TSOM method, wherein each step can be automated once the library is generated. In the case presented here, the library has only four major types of D-TSOM images. For other cases, there may be more or less major types of D-TSOM images in the library. However, we expect the same type of procedure to work for 3D shape process control of many types of shapes and target sizes, ranging from micro-scale to nano-scale targets.

4. Conclusion

In this paper, we have shown how TSOM could be applied in a high-volume manufacturing environment by using numerical signatures from measured D-TSOM images that have been developed into a reference library or database. Thus, we have proposed and demonstrated a low-cost, high-throughput, and nondestructive 3D shape process monitoring method for truly 3D or HAR type of targets using conventional optical microscopes. This tool can fill the gap by satisfying the HVM metrology needs of not only HAR but also other types of truly 3D targets for which 3D shape process control/monitoring is needed. This work indicates that targets with surfaces hidden from the direct illumination could also be analyzed using TSOM. We have also pointed out that TSOM has unique advantages over other metrologies such as scatterometry, and SEM.

Acknowledgment

We thank Dr John Kramar for his suggestions, and Dr Emil Agocs for his help.

ORCID iDs

Ravi Kiran Attota https://orcid.org/0000-0002-0729-2435

References

[1] Postek M H and Hocken R J 2004 Instrumentation and metrology for nanotechnology *National Nanotechnology Initiative Workshop Report* (https://www.nano.gov/sites/default/files/pub_resource/nni_instrumentation_metrology_rpt.pdf)

[2] Picotto G B, Koenders L and Wilkening G 2009 Nanoscale metrology *Meas. Sci. Technol.* **20** 080101

[3] Leach R K *et al* 2011 The European nanometrology landscape *Nanotechnology* **22** 122001

[4] Häusler G and Ettl S 2011 Limitations of optical 3D sensors *Optical Measurement of Surface Topography* ed R Leach (Berlin: Springer) pp 23–48

[5] Zhang X *et al* 2014 Addressing FinFET metrology challenges in 1 × node using tilt-beam critical dimension scanning electron microscope *J. Micro/Nanolith. MEMS MOEMS* **13** 041407

[6] Schulmeyer I, Lechner L, Gu A, Estrada R, Stewart D, Stern L, McVey S, Goetze B, Mantz U and Jammy R 2016 Advanced metrology and inspection solutions for a 3D world *2016 Int. Symp. on VLSI Technology, Systems and Application (VLSI-TSA) (25–27 April 2016)* pp 1–2

[7] Arceo A, Bunday B, Cordes A and Vartanian V 2012 Evolution or revolution: the path for metrology beyond the 22 nm node *Solid State Technol.* **55** 15–9

[8] Crimmins T F 2010 Defect metrology challenges at the 11 nm node and beyond *Proc. SPIE* **7638** 76380H

[9] Takamasu K, Iwaki Y, Takahashi S, Kawada H, Ikota M, Lorusso G F and Horiguchi N 2016 3D-profile measurement of advanced semiconductor features by reference metrology *Proc. SPIE* **9778** 97781T

[10] Attota R, Silver R and Barnes B M 2008 Optical through-focus technique that differentiates small changes in line width, line height and sidewall angle for CD, overlay, and defect metrology applications *Proc. SPIE* **6922** 69220E

[11] Vaid A, Elia A, Iddawela G, Bozdog C, Sendelbach M, Kang B C, Isbester P K and Wolfling S 2014 Hybrid metrology: from the lab into the fab *MOEMS* **13** 041410

[12] Bunday B 2016 HVM metrology challenges towards the 5 nm node *Proc. SPIE* **9778** 97780E

[13] Bunday B, Germer T A, Vartanian V, Cordes A, Cepler A and Settens C 2013 Gaps analysis for CD metrology beyond the 22 nm node *Proc. SPIE* **8681** 86813B

[14] Allen R A, Vartanian V, Read D and Baylies W 2014 Metrology for 3D integration *ECS Trans.* **61** 105–12

[15] Vartanian V, Allen R A, Smith L, Hummler K, Olson S and Sapp B 2014 Metrology needs for through-silicon via fabrication *J. Micro/Nanolith. MEMS MOEMS* **13** 011206

[16] Jo T, Kim S and Pahk H 2013 3D measurement of TSVs using low numerical aperture white-light scanning interferometry *J. Opt. Soc. Korea* **17** 317–22

[17] Ku Y S, Shyu D M, Hsu W T, Chang P Y, Chen Y C and Pang H L 2011 3D interconnect metrology in CMS/ITRI *Proc. SPIE* **8082** 80820I

[18] Attota R, Dixson R G, Kramar J A, Potzick J E, Vladar A E, Bunday B, Novak E and Rudack A 2011 TSOM Method for semiconductor metrology *Proc. SPIE* **7971** 79710T

[19] Schroettner H, Schmied M and Scherer S 2006 Comparison of 3D surface reconstruction data from certified depth standards obtained by SEM and an infinite focus measurement machine (IFM) *Microchim. Acta* **155** 279–84

[20] Punge A, Rizzoli S O, Jahn R, Wildanger J D, Meyer L, Schonle A, Kastrup L and Hell S W 2008 3D reconstruction of high-resolution STED microscope images *Microsc. Res. Tech.* **71** 644–50

[21] Wildanger D, Medda R, Kastrup L and Hell S W 2009 A compact STED microscope providing 3D nanoscale resolution *J. Microsc.* **236** 35–43

[22] Cuijpers V M J I, Walboomers X F and Jansen J A 2011 Scanning electron microscopy stereoimaging for three-dimensional visualization and analysis of cells in tissue-engineered constructs: technical note *Tissue Eng.* C **17** 663–8

[23] Kramar J A, Dixson R and Orji N G 2011 Scanning probe microscope dimensional metrology at NIST *Meas. Sci. Technol.* **22** 052002

[24] Orji N G, Dixson R G, Vladar A E and Postek M T 2011 Strategies for nanoscale contour metrology using critical dimension atomic force microscopy *Proc. SPIE* **8105** 810505

[25] Carrero J and Percin G 2012 Accurate optical CD profiler based on specialized finite element method *Proc. SPIE* **8324** 83240P

[26] Dai G L, Hassler-Grohne W, Huser D, Wolff H, Fluegge J and Bosse H 2012 New developments at Physikalisch Technische Bundesanstalt in three-dimensional atomic force microscopy with tapping and torsion atomic force microscopy mode and vector approach probing strategy *J. Micro/Nanolith. MEMS MOEMS* **11** 011004

[27] Kopek B G, Shtengel G, Xu C S, Clayton D A and Hess H F 2012 Correlative 3D superresolution fluorescence and electron microscopy reveal the relationship of mitochondrial nucleoids to membranes *Proc. Natl Acad. Sci. USA* **109** 6136–41

[28] Vladar A E, Cizmar P, Villarrubia J S and Postek M T 2012 Can we get 3D CD metrology right? *Proc. SPIE* **8324** 832402

[29] Li J, Kritsun O, Dasari P, Volkman C, Wallow T and Hu J T 2013 Evaluating scatterometry 3D capabilities for EUV *Proc. SPIE* **8681** 86810S

[30] Qin J, Silver R M, Barnes B M, Zhou H and Goasmat F 2013 Fourier domain optical tool normalization for quantitative parametric image reconstruction *Appl. Opt.* **52** 6512–22

[31] Sunday D F, Hammond M R, Wang C Q, Wu W L, Kline R J and Stein G E 2013 Three-dimensional x-ray metrology for block copolymer lithography line-space patterns *J. Micro/Nanolith. MEMS MOEMS* **12** 031103
[32] Yamaguchi A, Ohashi T, Kawasaki T, Inoue O and Kawada H 2013 Three-dimensional profile extraction from CD-SEM image and top/bottom CD measurement by line-edge roughness analysis *Proc. SPIE* **8681** 86812Z
[33] Chao R, Kohli K K, Zhang Y L, Madan A, Muthinti G R, Hong A J, Conklin D, Holt J and Bailey T C 2014 Multitechnique metrology methods for evaluating pitch walking in 14 nm and beyond FinFETs *J. Micro/Nanolith. MEMS MOEMS* **13** 041411
[34] Guo H X, Itoh H, Wang C M, Zhang H and Fujita D 2014 Focal depth measurement of scanning helium ion microscope *Appl. Phys. Lett.* **105** 023105
[35] Ku Y S 2014 Spectral reflectometry for metrology of three-dimensional through-silicon vias *J. Micro/Nanolith. MEMS MOEMS* **13** 011209
[36] Silver R M, Barnes B M, Zhang N F, Zhou H, Vladar A, Villarrubia J, Kline J, Sunday D and Vaid A 2014 Optimizing hybrid metrology through a consistent multi-tool parameter set and uncertainty model *Proc. SPIE* **9050** 905004
[37] Vladar A E, Villarrubia J S, Chawla J, Ming B, Kline J R, List S and Postek M T 2014 10 nm three-dimensional CD-SEM metrology *Proc. SPIE* **9050** 90500A
[38] Attota R, Silver R M, Bishop M R and Dixson R G 2006 Optical critical dimension measurement and illumination analysis using the through-focus focus metric *Proc. SPIE* **6152** 61520K
[39] Attota R, Silver R M, Stocker M, Marx E, Jun J, Davidson M and Larrabee R 2003 A new method to enhance overlay tool performance *Proc. SPIE* **5038** 428–36
[40] Orji N G, Dixson R G, Ng B P, Vladar A E and Postek M T 2016 Contour metrology using critical dimension atomic force microscopy *J. Micro/Nanolith. MEMS MOEMS* **15** 83240U
[41] Heurlin M, Anttu N, Camus C, Samuelson L and Borgström M T 2015 *In situ* characterization of nanowire dimensions and growth dynamics by optical reflectance *Nano Lett.* **15** 3597–602
[42] Vaid A *et al* 2011 A holistic metrology approach: hybrid metrology utilizing scatterometry, CD-AFM, and CD-SEM *Proc. SPIE* **7971** 797103
[43] Association S I 2016 *The International Technology Roadmap for Semiconductors (ITRS)* (San Jose: Semiconductor Industry Association) (http://www.itrs2.net/itrs-reports.html)
[44] IEEE 2018 *International Roadmap for Devices and Systems 2017 Edition: Metrology* (IEEE) (https://irds.ieee.org/images/files/pdf/2017/2017IRDS_MET.pdf)
[45] Cunf D L, Höglund L J and Laurent N 2011 In-line metrology of high aspect ratio structu with MBIR technique *2011 IEEE/SEMI Advanced Semiconductor Manufacturing Conf. (16–18 May 2011)* pp 1–5
[46] Attota R, Germer T A and Silver R M 2008 Through-focus scanning-optical-microscope imaging method for nanoscale dimensional analysis *Opt. Lett.* **33** 1990–2
[47] Attota R and Silver R 2011 Nanometrology using a through-focus scanning optical microscopy method *Meas. Sci. Technol.* **22** 02402
[48] Attota R, Bunday B and Vartanian V 2013 Critical dimension metrology by through-focus scanning optical microscopy beyond the 22 nm node *Appl. Phys. Lett.* **102** 02402
[49] Ryabko M, Koptyaev S, Shcherbakov A, Lantsov A and Oh S Y 2014 Motion-free all optical inspection system for nanoscale topology control *Opt. Express* **22** 14958–63
[50] Han S, Yoshizawa T, Zhang S, Lee J H, Park J H, Jeong D, Shin E J and Park C 2016 Tip/tilt-compensated through-focus scanning optical microscopy *Proc. SPIE* **10023** 100230P
[51] Taute K M, Gude S, Tans S J and Shimizu T S 2015 High-throughput 3D tracking of bacteria on a standard phase contrast microscope *Nat. Commun.* **6** 8776
[52] Attota R and Dixson R G 2014 Resolving three-dimensional shape of sub-50 nm wide lines with nanometer-scale sensitivity using conventional optical microscopes *Appl. Phys. Lett.* **105** 043101
[53] Arceo A, Bunday B, Vartanian V and Attota R 2012 Patterned defect & CD metrology by TSOM beyond the 22 nm node *Proc. SPIE* **8324** 83240E
[54] Park S-w, Park G, Kim Y, Cho J H, Lee J and Kim H 2018 Through-focus scanning optical microscopy with the Fourier modal method *Opt. Express* **26** 11649–57
[55] SEMI 2013 3D5-0613—Guide for Metrology Techniques to be Used in Measurement of Geometrical Parameters of Through-Silicon Vias (TSVs) in 3DS-IC Structures (SEMI)
[56] Attota R K and Kang H 2016 Parameter optimization for through-focus scanning optical microscopy *Opt. Express* **24** 14915–24
[57] Attota R 2016 Noise analysis for through-focus scanning optical microscopy *Opt. Lett.* **41** 745–8
[58] Attota R and Kramar J 2016 Optimizing noise for defect analysis with through-focus scanning optical microscopy *Proc. SPIE* **9778** 977811
[59] Attota R K, Weck P, Kramar J A, Bunday B and Vartanian V 2016 Feasibility study on 3D shape analysis of high-aspect-ratio features using through-focus scanning optical microscopy *Opt. Express* **24** 16574–85
[60] Gineste J M, Macko P, Patterson E A and Whelan M P 2011 Three-dimensional automated nanoparticle tracking using Mie scattering in an optical microscope *J. Microsc.* **243** 172–8
[61] Abrahamsson S 2013 Fast multicolor 3D imaging using aberration-corrected multifocus microscopy *Nat. Methods* **10** 60–3
[62] Attota R K 2018 Through-focus or volumetric type of optical imaging methods: a review *J. Biomed. Opt.* **23** 1–10